Silicon Dielectric Diplexer Module for 600-GHz-Band Frequency-Division Multiplexing Wireless Communication

Norihiko Shibata, *Student Member, IEEE*, Yuta Uemura, *Student Member, IEEE*, Yuma Kawamoto, Li Yi, *Member, IEEE*, Masayuki Fujita, *Member, IEEE*, and Tadao Nagatsuma, *Fellow, IEEE*

***Abstract*—We developed a silicon (Si) dielectric diplexer module for 600-GHz-band frequency-division multiplexing wireless communication. This diplexer was developed based on Si dielectric waveguide technology, which provides low-loss transmission characteristics compared with the conventional metallic terahertz-transmission platform, such as metallic hollow waveguides. It includes straight waveguides based on an effective medium composed of Si and air, and a coupler comprising of two adjacent unclad Si waveguides. Furthermore, for the communication system integration, we developed a practical and low-insertion loss module with WR1.5 metallic hollow waveguide input–output interfaces and modularized the diplexer. We performed transmission measurement experiments with the fabricated diplexer module and achieved 3-dB bandwidths of 101 and 37 GHz, and crosstalk of −34 dB at 680 GHz and −41 dB at 618 GHz in the cross and bar directions, respectively. Finally, we performed a two-channel wireless communication experiment using the developed diplexer module in the 600-GHz band. We achieved error-free communication at 10 and 6 Gbit/s on the cross and bar channels, respectively. In addition, we achieved a data rate of up to 12.5 Gbit/s at the forward error correction limits for both channels.**

***Index Terms*—600-GHz band, diplexer, frequency-division multiplexing (FDM), packaging, silicon (Si) dielectric waveguide, terahertz (THz) wireless communication.**

Manuscript received December 14, 2021; revised March 4, 2022; accepted March 31, 2022. Date of publication April 19, 2022; date of current version July 5, 2022. This work was supported in part by the Collaborative Research Based on Industrial Demand of the Japan Science and Technology Agency "Terahertz-wave: Towards Innovative Development of Terahertz-wave Technologies and Applications," in part by the Ministry of Internal Affairs and Communications, Japan, through the 2020 Strategic Information and Communications R&D Promotion Program (SCOPE) under Grant 195010002, in part by the Japan Science and Technology Agency through Core Research for Evolutional Science and Technology (CREST) program under Grant JPMJCR21C4, in part by the National Institute of Information and Communications Technology (NICT), Japan, through commissioned research under Grant 03001, in part by KAKENHI, Japan, under Grant 20H00249, and in part by the ONR Foreign Research under Grant N62909-18-1-2015. *(Corresponding authors: Norihiko Shibata; Yuta Uemura; Yuma Kawamoto; Li Yi; Masayuki Fujita; Tadao Nagatsuma.)*

The authors are with the Graduate School of Engineering Science, Osaka University, Osaka 560-8531, Japan (e-mail: u707852j@alumni.osaka-u.ac.jp; u402996g@alumni.osaka-u.ac.jp; u582868f@ecs.osaka-u.ac.jp; yi@ee.es.osaka-u.ac.jp; fujita@ee.es.osaka-u.ac.jp; nagatuma@ee.es.osaka-u.ac.jp).

Color versions of one or more figures in this article are available at https://doi.org/10.1109/TTHZ.2022.3167946.

Digital Object Identifier 10.1109/TTHZ.2022.3167946

I. Introduction

TERAHERTZ (THz) waves, whose frequencies range from 100 GHz to 10 THz, have attracted significant attention owing to their potential for high-speed wireless communication, due to its intrinsic broad bandwidth [1]–[4]. According to previous research, real-time error-free [bit error rate (BER) $< 10^{-11}$] wireless communication of 50 Gbit/s has been reported in the 300-GHz band with simple on–off keying modulation [5], [6]. To achieve further high-speed wireless communication, the 600-GHz band is most promising. The 600-GHz band has an atmospheric window of over 100 GHz [7], which indicates the frequency region where the atmospheric attenuation rate is low so that an ultrawide bandwidth can be available [8], [9]. An error-free wireless communication of 14.5 Gbit/s in the 600-GHz band using a unitraveling-carrier photodiode (UTC-PD) transmitter (Tx) [9] and a photonics-based heterodyne receiver (Rx) scheme has been reported [10].

Moreover, multiplexing technique is a promising method to expand the potential of THz wireless communication. Multiplexing can enhance the throughput of wireless communication by transmitting multiple individual carrier signals on a single shared transmission path. THz wireless communications are expected to be used for high-capacity multichannel communication in applications such as intervehicle communications [11], [12], indoor wireless communications [13], [14], and data center wireless links [15], and multiplexing plays an essential role in each of them. Multiplexing is classified in various ways such as time-division [16]–[18], mode-division [19]–[21], code-division [22]–[24], and polarization division [25]–[27]. Among them, the frequency-division multiplexing (FDM) method [28], which can separate and make effective use of a wide bandwidth, is most suitable for wireless communication in the THz band, especially in the 600-GHz band, which includes more than a 100-GHz atmospheric window.

To realize FDM wireless communication in the 600-GHz band, multiplexers are required to divide and combine carrier signals at the physical layer. However, at high frequencies of over the 600-GHz band, conventional transmission platforms such as metallic hollow waveguides, microstrip lines [29], and coplanar waveguides [30] suffer from increased transmission loss caused by skin effect and fabrication process errors [31], [32]. For example, the propagation loss of WR1.5 metallic

hollow waveguides has been experimentally reported to range between 1–2 dB/cm [33]. Recently, metallic hollow waveguides using micromachine process techniques [34]–[36], which offer high processing accuracy, have been developed to solve the abovementioned problem.

In this article, we report an alternative approach to realize multiplexers by using silicon (Si) dielectric waveguide technology [37]–[44] as an efficient passive platform with low-loss and broadband characteristics in the THz range. According to previous studies in the 300-GHz band, the propagation loss of Si dielectric waveguide technology has been reported to be less than 0.05 dB/cm in the operating band, with a bandwidth of 130 GHz and above [37], [42]. Additionally, functional components such as high-Q cavities for THz sensors [39] and THz absorbers [45] using photonic crystals and planar antennas [46] using multiple taper structures have been demonstrated. In particular, multiplexers [43] using unclad and effective medium Si waveguides are promising for 600-GHz-band FDM wireless communication.

However, there are two challenges in realizing FDM communication using Si dielectric waveguide technology. The first is the lack of a packaging technique for Si dielectric waveguide technology. Until now, intricate alignments using tweezers have been performed in laboratory experiments, as shown in [40], [41], and [43]. In addition, the exposed Si dielectric devices are fragile and difficult to handle owing to their submillimeter thickness, which is not practical for system applications.

The other is the crosstalk between the channels in Si dielectric multiplexers causes a performance deterioration in multichannel simultaneous transmission. Therefore, the previous study [43] has only been successful in the transmission for each channel separately.

In this study, we designed an Si diplexer and Si dielectric waveguide packaging module and demonstrated their operation through transmission measurements and wireless communication experiments. In Section II, we developed an Si dielectric waveguide module with WR1.5 metallic hollow waveguide input–output (I/O) interfaces and measured it using a transmittance measurement experiment. In Section III, employing Si dielectric waveguide technology, we designed an Si dielectric diplexer, which is a key constituent of FDM communications in the 600-GHz band. To improve the crosstalk of the diplexer in accordance with the bandwidth available for wireless communication, we designed a coupler with an optimum coupling length and separation. Afterward, in Section IV, we describe the development of a 600-GHz-band two-channel wireless communication system using the developed Si diplexer module designed in Sections II and III and demonstrate its operation.

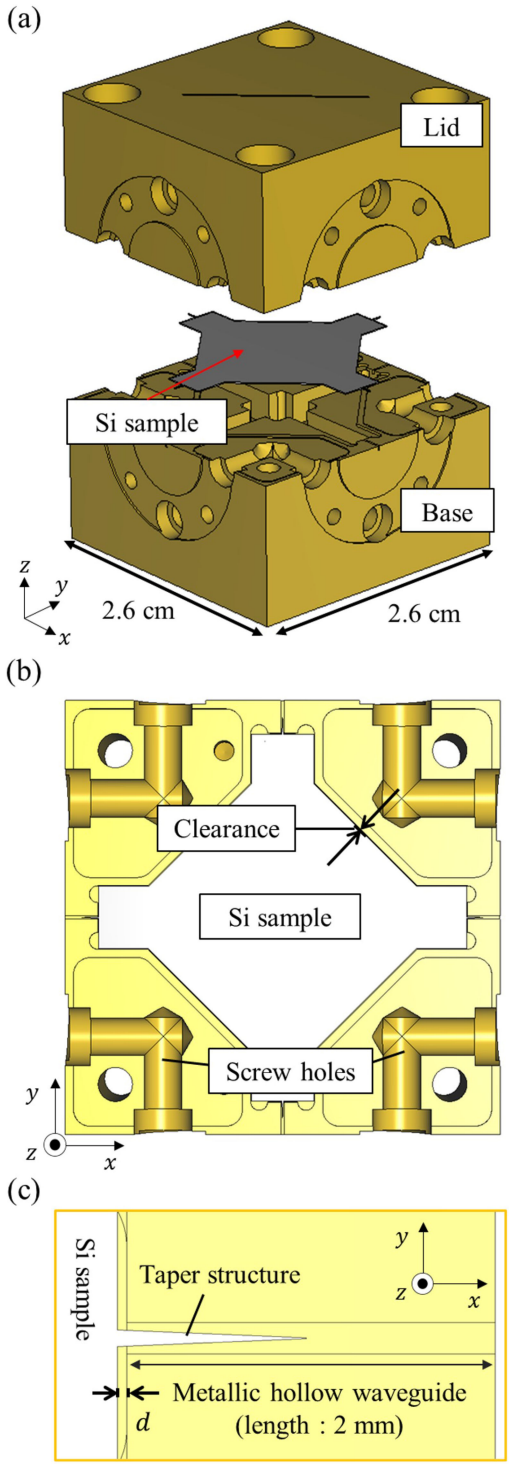

Fig. 1. Si dielectric waveguide packaging module. (a) Overview. (b) Top view of the base. (c) Connection between the taper structure of Si sample and module.

II. Si Dielectric Waveguide Packaging Module

A. Design

Initially, we developed a packaging module to establish a way of mounting Si dielectric waveguides, including a diplexer for FDM wireless communication. The design of the Si dielectric waveguide packaging module is illustrated in Fig. 1(a). The module has a cubic structure of 26 mm on each side. This module consists of two parts, the base and lid, and when in use, the lid is tightened and screwed on. As shown in Fig. 1(b), the base has a rhombus-like groove carved into it to avoid collision with the screw holes, which are used for connections to the metallic hollow waveguide. An Si sample for the 600-GHz-band Si dielectric waveguide, which has the same shape as that of the groove and a thickness of 100 μm, can be inserted. Any Si dielectric component can be utilized by adapting it to the standardized sample geometry. The clearance between the edge

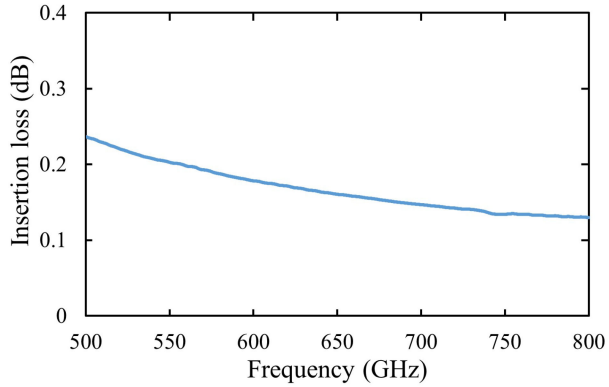

Fig. 2. Simulated insertion loss of the designed packaging module.

of the module groove and the Si sample was set to 25 μm, which is sufficient to hold the sample in the xy-plane. Therefore, when the Si sample was inserted into the module, the xy-plane alignment was automatically completed and the connection with the I/O port of the module was fixed in the best position. In the vicinity of the electromagnetic wave propagation area of the Si sample, sufficiently deep grooves of 3000 μm depth were carved into the base as well as the lid to prevent interference with the electromagnetic wave propagation.

Each of the four sides of this module has a WR1.5 metallic hollow waveguide I/O interface, which allows connections to other metallic hollow waveguide-based components such as THz sources, detectors, and amplifiers. The taper structure of the Si sample, whose length is 1 mm, provides a highly efficient connection of electromagnetic waves between the Si dielectric components and metallic hollow waveguide interfaces, as shown in Fig. 1(c). The taper insertion depth d was adjusted with a three-dimensional (3-D) full-wave simulation using CST Microwave Studio 2020 and determined to be 50 μm to achieve the best transmission characteristics. To achieve a low insertion loss, we minimized the length of the I/O metallic hollow waveguide in the module to 2 mm. Then, we compared the simulated characteristics of the Si dielectric straight waveguide with and without the module, and calculated the insertion loss of the module, as shown in Fig. 2. To take into account the material loss due to metal, the material of the packaging module in the simulation is gold (electric conductivity: 4.56×10^7 S/m). The insertion loss was found to be between 0.15–0.25 dB in the frequency range of 500–800 GHz, and this does not compromise the low-loss capability of the Si dielectric waveguides. The reason for the slightly higher insertion loss at low frequency is ascribed to the increased loss in the vicinity of the cutoff frequency of fundamental mode (TE10 mode) of the WR1.5 metallic hollow waveguide interfaces. Hence, it was concluded that the low-loss property of the Si dielectric waveguides was maintained in the proposed module.

B. Fabrication

Fig. 3(a) shows the fabricated packaging module for Si dielectric waveguides. The material used for the module was gold-plated tellurium copper. The fabrication error of the metallic

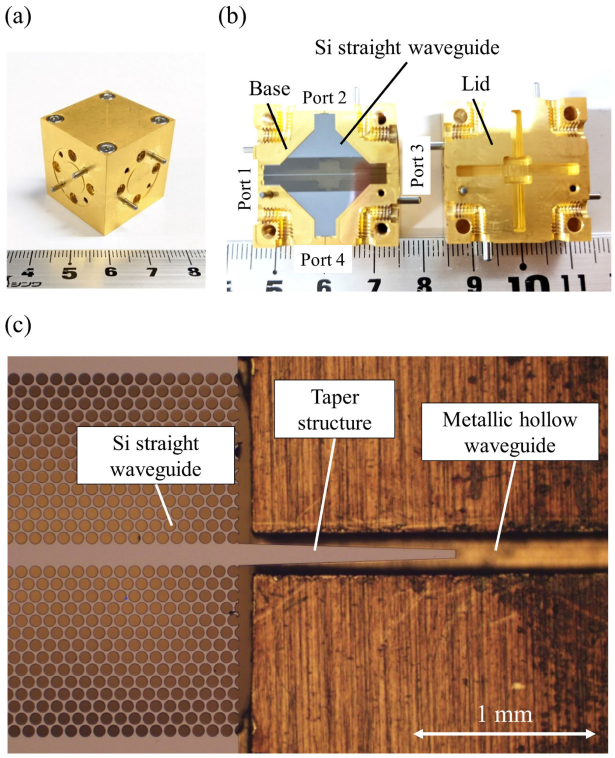

Fig. 3. Fabricated packaging module. (a) Overview. (b) View of the base and lid when Si straight waveguide is mounted. (c) Magnified photograph of the vicinity of the taper structure insertion area.

hollow waveguide part was approximately ±10 μm, and that of the other metallic parts was approximately ±20 μm.

In addition, a straight Si waveguide was fabricated to fit the rhombus-like groove of this module to estimate its performance, as shown in Fig. 3(b). This Si dielectric straight waveguide was fabricated on a 100-μm thick high-resistivity Si substrate (resistivity: 10 k Ω-cm, relative permittivity ϵ_r: 11.7) using a deep reactive ion etching (DRIE) process. The thickness of the Si substrate of the waveguide was set to 100 μm to operate in the 600-GHz band. This was based on the scaling law because previous studies have reported that the Si dielectric waveguides with a thickness of 200 μm operated in the 300-GHz band [37]. The fabricated straight waveguide has a line width of 100 μm and is surrounded by a hexagonal lattice periodic cylindrical hole array based on the Maxwell–Garnett effective medium approximation theory [41], [47], with a period of 65 μm and a diameter of 55 μm. As shown in Fig. 3(c), the taper structure of the Si dielectric straight waveguide is inserted parallel to the metallic hollow waveguide section of the packaging module, indicating good fabrication accuracy. The THz waves in the waveguide are confined by the total internal reflection between the effective medium and the waveguide core in-plane, and between the air and the waveguide core out-of-plane, and propagates with low-loss. The length of the tapering structure was 1000 μm. These taper structures become narrower at the ends, and the electromagnetic waves from the Si straight waveguides are gradually converted to propagation modes of the metallic hollow waveguide and coupled.

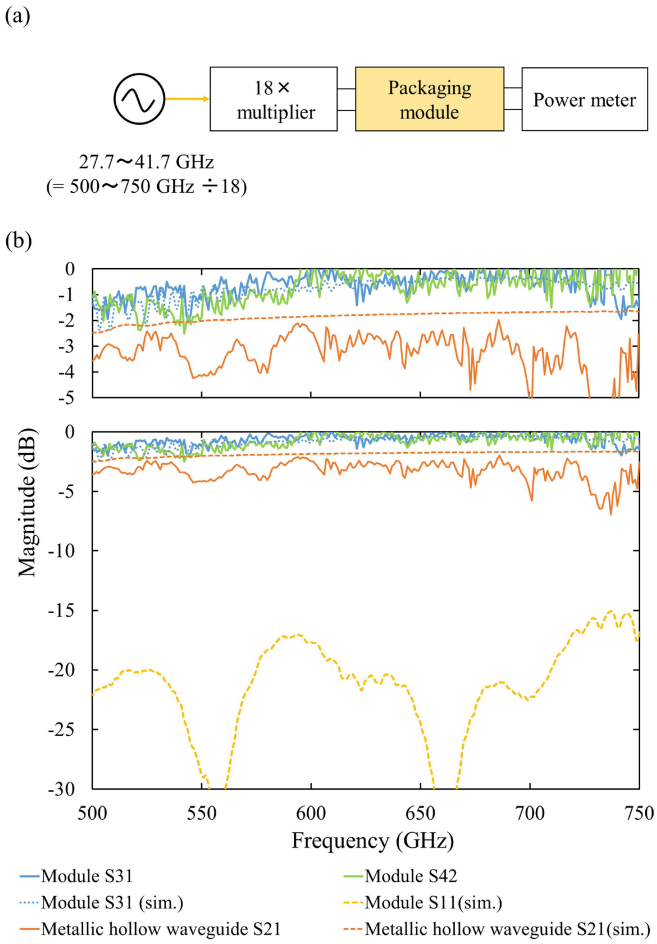

Fig. 4. Evaluation of the designed packaging module. (a) Block diagram of the evaluation experiment system. (b) Measured and calculated transmission characteristics of the module when Si straight waveguide is packaged, and metallic hollow waveguide with a length approximately equal to the module. Blue, green, yellow, and orange lines denote S31, S42, S11 of the Si module and S21 of the metallic hollow waveguide, respectively. Solid and dashed lines denote experimental and simulation, respectively. The vertical axis range in the upper figure is set from 0 to −5 dB, and the lower figure is set from 0 to −30 dB.

C. Characterization

The transmittance measurement system used to measure the module is shown in Fig. 4(a). An 18× multiplier was applied to generate THz waves ranging from 500 to 750 GHz by multiplying the signal from a millimeter-wave signal generator (SG). The generated THz waves were injected into the module packaged with an Si straight waveguide, which was directly connected to the metallic hollow waveguide interface of the 18× multiplier. Then, the output signal from the module was measured using a power meter (PM5, Virginia Diodes Inc.). The transmittance of the module was calculated from the measured power difference measured back to back. To demonstrate the operation in the two straight-line directions of the module (ports 1–3 and ports 2–4), we measured the transmittance of the Si straight waveguide mounted along each direction.

As shown in Fig. 4(b), the measured transmittances for S31 and S42 in the two directions were in good agreement with the simulated ones, and the 3-dB transmission bandwidth was greater than 250 GHz, indicating that the module was operating properly. In addition, the reflection coefficient for S11 of the module was analytically shown to be less than –15 to –20 dB for all the bands, which indicated that good transmission characteristics could be expected. As shown in Fig. 4(b), the experimental characteristics are in good agreement with the simulations, and the 3-dB transmission bandwidth is over 250 GHz, indicating that the module is operating properly. Furthermore, in order to compare a module fabricated using the conventional technique, we measured a straight metallic hollow waveguide with the same length (approximately 2.5 cm). These were fabricated by the same manufacturer using the same metal and plating material. As shown in Fig. 4(b), the measurement results for the straight metallic hollow waveguide were significantly degraded compared with the simulation results because of the effects of processing errors and scratches on the metal parts, as well as the energy loss caused by the skin effect.As the skin effect was larger at higher frequencies, the negative effect of the characteristic degradation was more pronounced at higher frequencies. The transmittance of the module with the Si straight waveguide was approximately 2–3 dB higher than that of a conventional metallic hollow straight waveguide, which demonstrates the superiority of the proposed Si dielectric waveguide packaging module with respect to transmission loss.

III. 600-GHz-Band Si Dielectric Diplexer

A. Configuration

Fig. 5(a) shows a photograph of the designed Si dielectric diplexer. As with the Si straight waveguide in the previous section, the diplexer is fabricated from a 100-μm-thick high-resistivity Si substrate (resistivity: $<$10 kΩ-cm, relative permittivity ϵ_r: 11.7) using the DRIE process. The diplexer is composed of four straight waveguides, taper structures, and a coupler, as shown in Fig. 5(b)–(d). The parameters (e.g., line widths, radius, and period of hole array) of the straight waveguide and the taper structure are the same as those of the Si dielectric straight waveguide described in Section II. As shown in Fig. 5(c), the taper structures are installed at the edge of each straight waveguide part to provide an I/O interface to the WR1.5 metallic hollow waveguide. In the center of the diplexer, we implemented an evanescent coupler made of two adjacent Si unclad waveguides, which were inclined at 60°. The straight waveguides and couplers are joined by bent unclad waveguides. In addition, its shape is designed to match the rhombus-like groove shape of the packaging module as described in the previous section.

B. Selection of Operation Frequency

To determine the appropriate operating frequency for the diplexer, we conducted frequency selection experiments using a 600-GHz-band wireless communication system [10], as shown in Fig. 6. On the Tx side, the pseudorandom binary sequence (PRBS) of the $2^9 - 1$ data stream from the pulse pattern generator (PPG) was applied to the electro-optic amplitude modulator (EOAM), which modulated the optical signals from a wavelength-tunable laser pair. The frequency difference

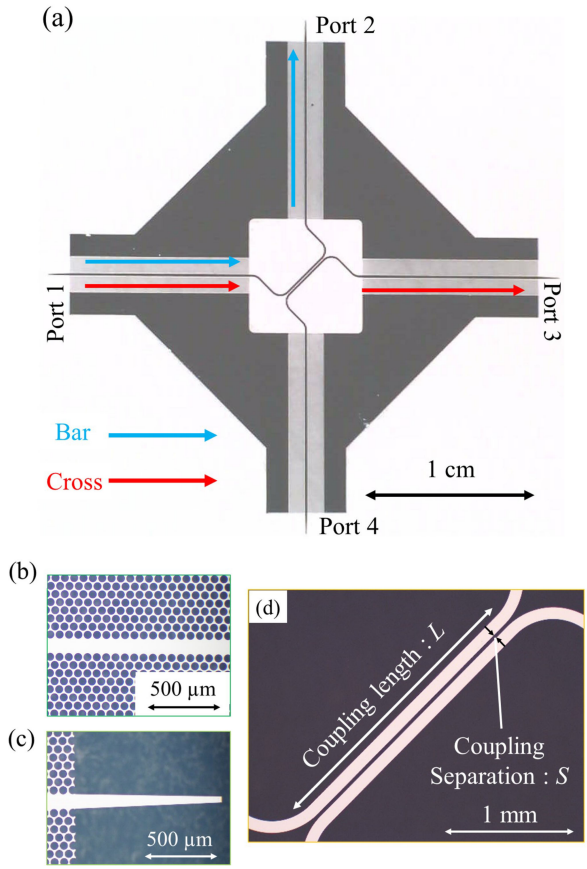

Fig. 5. Fabricated Si dielectric diplexer. (a) Overview. (b) Straight waveguide part. (c) Taper structure part. (d) Coupler part.

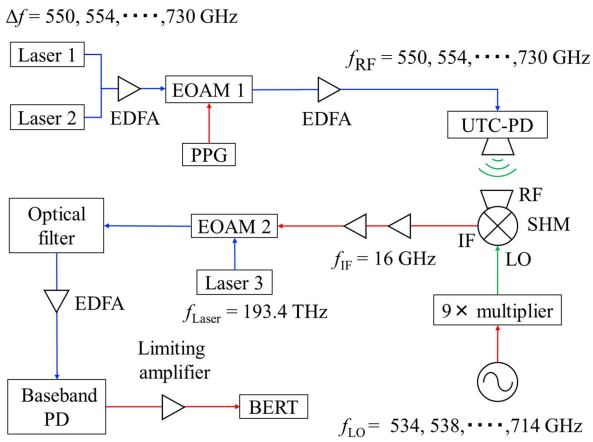

Fig. 6. Block diagram of experimental system for 600-GHz-band wireless communication to determine operation frequency bands. Blue, red, and green line denotes optical signal, electric signal, and THz signal, respectively. EDFA: erbium doped fiber amplifier. PPG: pulse pattern generator. EOAM: electro-optic amplitude modulator. UTC-PD: unitraveling carrier photodiode. SHM: sub-harmonic mixer. BERT: bit error rate tester.

of the wavelength-tunable laser pair was changed from 550 to 730 GHz in 4-GHz intervals. Then, the two modulated optical signals were injected into the UTC-PDs as Txs, and the photomixing phenomenon [48] generated a modulated THz wave with a center frequency of 550–730 GHz, corresponding to the different frequencies of the wavelength-tunable laser pair. The

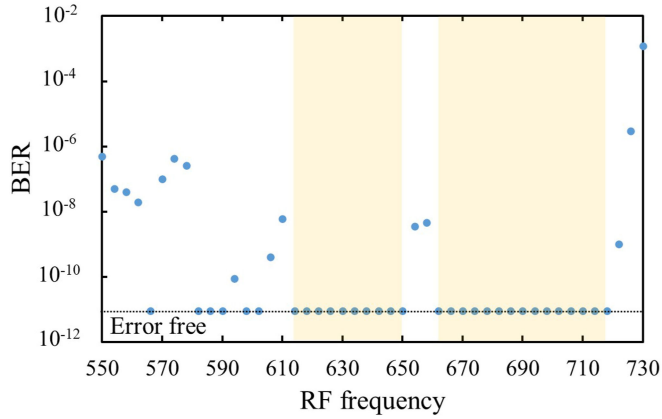

Fig. 7. Experimental plots of RF carrier frequency vs. BER characteristics at a data rate of 6 Gbit/s in the 600-GHz band. The orange area indicates the frequency band where error-free wireless communication is satisfied at a data rate of 6 Gbit/s.

THz wave radiated from a horn antenna, which was attached to the UTC-PD, and were received by the sub-harmonic mixer (SHM). On the Rx side, we employed an optical intermediate frequency (IF) Rx scheme [10], [49]. The SHM is pumped by the local oscillator (LO) signal, which is multiplied by a signal from a millimeter-wave SG with an IF frequency of 16 GHz. That is, when the radio frequency (RF) frequency is 550 GHz, the LO frequency should be set to 534 GHz through the 9× multiplier and down-convert the RF signal to the IF signal. The IF signal was amplified by two baseband amplifiers and then up-converted by EOAM to a single-mode optical signal with a center frequency of 193.4 THz. The EOAM bias is set to the null point to cut off the sideband signal, either the lower or upper side bands, with the center carrier signal from the laser suppressed. The IF signal filtered by the optical bandpass filter, which has rolloff characteristics of 3.2 dB/GHz in the 1.55-μm band, is detected by a baseband photodiode (PD) to obtain and demodulate the data signal. The BER characteristics at each RF frequency from 550 to 730 GHz were measured with a bit error rate tester (BERT) after waveform shaping of the demodulated signal with a limiting amplifier.

Fig. 7 shows the RF frequency and BER characteristics at a data rate of 6 Gbit/s applied from PPG in a 600-GHz-band wireless communication system. In the current wireless communication system, the frequency bands where 6-Gbit/s error-free communication is possible is limited to approximately 615–650 GHz and 670–710 GHz. This is caused by the limitation of output power from UTC-PD [9] and the lack of sensitivity of SHM in the 600-GHz band. Hence, the Si dielectric diplexer to be designed must match the broadband and small crosstalk frequency characteristic region of these bands that are available for uncongested FDM wireless communications.

C. Design

To achieve FDM communications in the 600-GHz band, we adjust the coupler coupling length L and coupling spacing S to align the bandwidth and low-crosstalk frequency band of the diplexer with the bandwidth of the previous subsection (i.e.,

615–650 GHz and 670–710 GHz). In general, the electromagnetic waves propagating on two parallel tracks take on two different supermodes, odd and even, each with a different phase constant, β_{odd} and β_{even} [50]. If there is no difference between the two phase constants (i.e., $\beta_{\text{odd}} = \beta_{\text{even}}$), the two modes will propagate in the bar direction without being transferred to the adjacent waveguide in step. However, if there is a finite difference between the two phase constants (i.e., $\beta_{\text{odd}} \neq \beta_{\text{even}}$), the energy gradually leaks into the adjacent waveguide, and when the two phase constants reach π radians, all the energy is transferred in the cross direction. In general, we can express the relationship between the lowest order coupling length L and the two propagation constants for power transfer in the cross direction in the following equation:

$$L = \frac{\pi}{|\beta_{\text{odd}} - \beta_{\text{even}}|}. \tag{1}$$

Equation (1) is also synonymous with the minimum state of L, where all the powers propagate in the cross direction, and this state is repeated for odd multiples of length L.

To determine the optimum coupling length L and separation S, the relationship between the center frequency of the electromagnetic wave propagating in the cross direction and parameters L and S were investigated using 3-D full-wave simulation, as shown in Fig. 8(a) and (b). As the coupling length L is increased, the center frequency in the cross direction and bar direction shifts to the high-frequency side, respectively. It can also be noted that as the coupling separation S is increased, the electromagnetic coupling between adjacent waveguides becomes weaker, and thus a longer coupling length L is required in both directions. It should be noted that by adjusting coupling length L and separation S, the center frequency can be varied from 550 to 800 GHz in both the bar and cross directions, indicating that the diplexer can adjust the separation band to match any frequency band in the 600-GHz band.

In addition, Fig. 8(b) shows the simulated relationship between the relative bandwidth in the cross direction, coupling length L of the coupler, and the coupling separation S. This graph shows that a long coupling length L and narrow coupling separation S are effective in achieving a wide relative bandwidth. However, if the coupling separation S is too small, the center frequency will be shifted significantly owing to a dimension error of approximately ± 10 μm in the DRIE fabrication process. Furthermore, the long coupling length L makes the area of the diplexer very large, making it difficult to pack the module. Taking the abovementioned points into account, we eventually set the coupler parameters to a coupling length L of 2275 μm and a coupling separation S of 33 μm so that the center frequency in the cross direction and bar direction is 680 and 618 GHz, respectively.

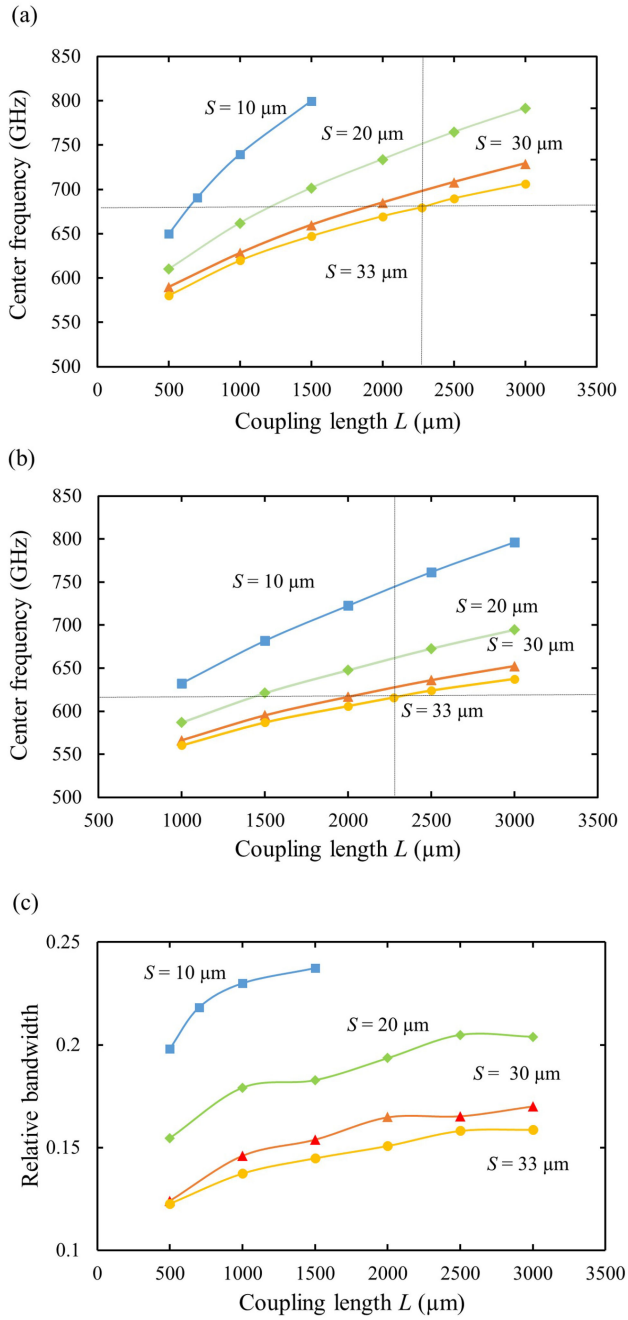

Fig. 8. Simulation of coupler characteristics with various coupling length L and coupling separations S. Blue, green, red, and orange denote $S = 10$, 20, 30, and 33 μm, respectively. (a) Relationship between center frequency of the THz waves propagating in cross direction and coupling length L. (b) Relationship between center frequency of the THz waves propagating in bar direction and L. (c) Relationship between the relative bandwidth of THz waves propagating in cross direction and L.

D. Characterization

As shown in Fig. 9(a), the S-parameters of the diplexer packaged in the developed module were acquired from the 3-D full-wave simulation and experiment using the transmittance measurement system shown in Fig 3(c) in the frequency range of 575–800 GHz. The experimental and simulated characteristics are in good agreement. We experimentally achieved 3-dB transmission bandwidths of 101 and 37 GHz in the cross (from port 1 to port 3) and the bar (from port 1 to port 2) directions, respectively. The maximum transmittance of –0.24 and –1.08 dB was achieved in the cross and bar directions, respectively.

Next, we define crosstalk $= -|\text{S31–S21}|$ from the experimental transmission characteristics in Fig. 9(a), and plot the

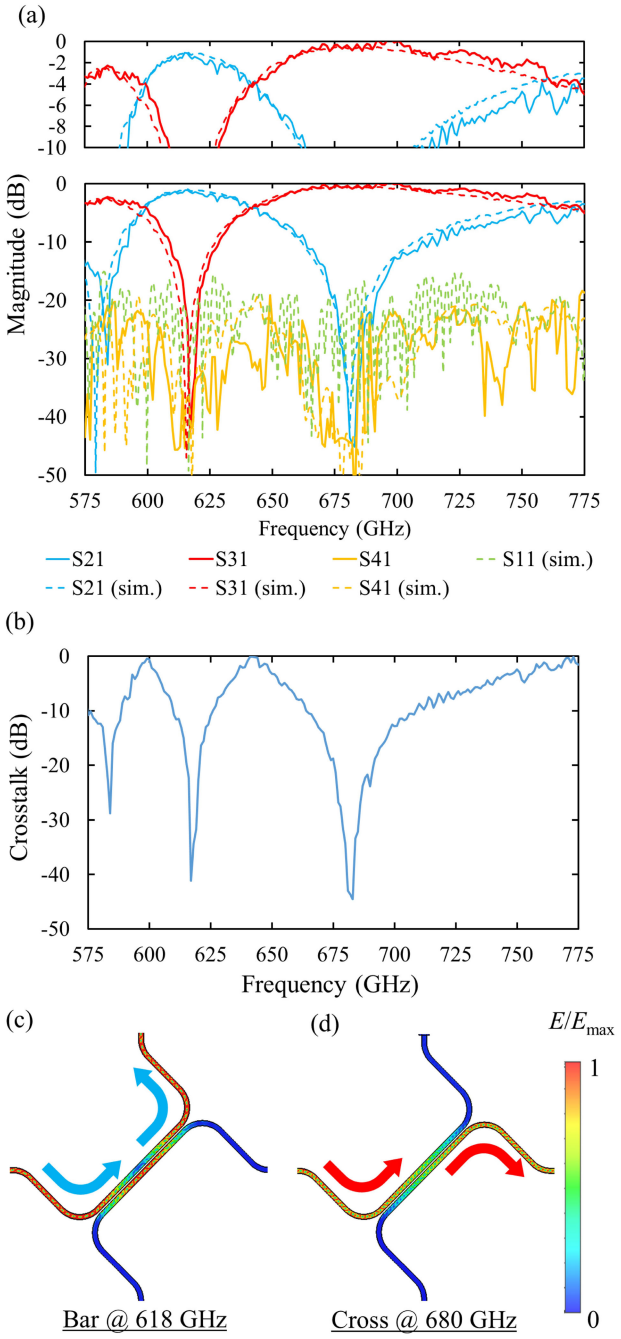

Fig. 9. Characteristics of the designed Si dielectric diplexer. (a) Measured (solid lines) and simulated (dashed lines) *S*-parameter of Si dielectric diplexer packaged by the module. The vertical axis range in the upper figure is set from 0 to −10 dB, and the lower figure is set from 0 to −50 dB. Green, blue, red, and orange denote S11, S21, S31, and S41, respectively. (b) Crosstalk of Si dielectric diplexer calculated from experimental transmission characteristics. Crosstalk = −|S31–S21|. (c) Simulated electric-field intensity distribution at 618 GHz propagating in the bar direction. (d) Simulated electric-field intensity distribution at 680 GHz propagating in the cross direction.

relationship between frequency and crosstalk in Fig. 9(b) We achieved crosstalk values of –34 dB and –41 dB at frequencies of 618 and 680 GHz, respectively. We expect that by setting these frequencies as the carrier frequency in FDM wireless communication, the low crosstalk of the diplexer can prevent interference between channels. As shown in the electric field distribution in

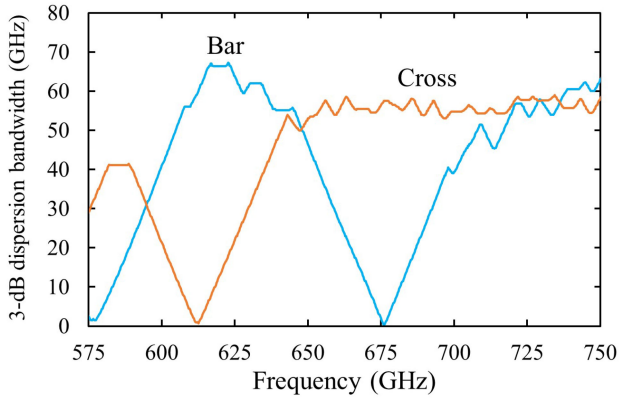

Fig. 10. Simulated 3-dB dispersion bandwidth of Si dielectric diplexer. Blue and orange denote bar and cross direction, respectively.

Fig. 9(c) and (d) at 618 and 680 GHz, the THz wave propagates in the bar and cross directions, respectively, without leaking to other ports. Furthermore, S11, which indicates the reflection coefficient, and S41, which is the transmission to a port not in use, are both less than approximately –20 dB.

In addition, as shown in Fig. 10, we calculated the 3-dB dispersion bandwidth [38] of the designed diplexer, which means that the 3-dB bandwidth is limited by the group delay dispersion, given by the group velocity which was obtained from the 3-D full-wave simulation. The 3-dB dispersion bandwidth at 680 GHz in the cross direction and 618 GHz in the bar direction are 56 and 66 GHz, respectively, which are much higher than the current maximum wireless transmission data rate of 14.5 Gbit/s in the 600-GHz band [10]. This indicates that the influence of the insertion of the diplexer module on the quality of communication is negligible.

IV. 600-GHz-Band Two-Channel Wireless Communication With Si Dielectric Diplexer Module

A. Experimental System

To demonstrate the THz-wave combining operation of the developed Si diplexer module in a wireless communication system and the possibility of FDM wireless communication, we performed a two-channel wireless communication experiment using the developed diplexer module in the 600-GHz band. Fig. 11(a) shows a block diagram of the experimental setup for a 600-GHz-band two-channel wireless communication system with an Si diplexer module.

On the Tx side, we employed two UTC-PDs for two-channel wireless communications. The PRBS of the $2^9 - 1$ data stream from the PPG was applied to two EOAMs, which modulated the optical signals from two wavelength-tunable laser pairs with frequency differences of 680 and 618 GHz, respectively. Then, the two modulated optical signals are injected into two UTC-PDs used as Txs, which generate modulated THz waves with center frequencies of 680 and 618 GHz by the photomixing phenomenon [48]. The THz waves in the cross and bar directions emitted from UTC-PD 1 (center frequency: 680 GHz) and UTC-PD 2 (center frequency: 618 GHz), respectively, were

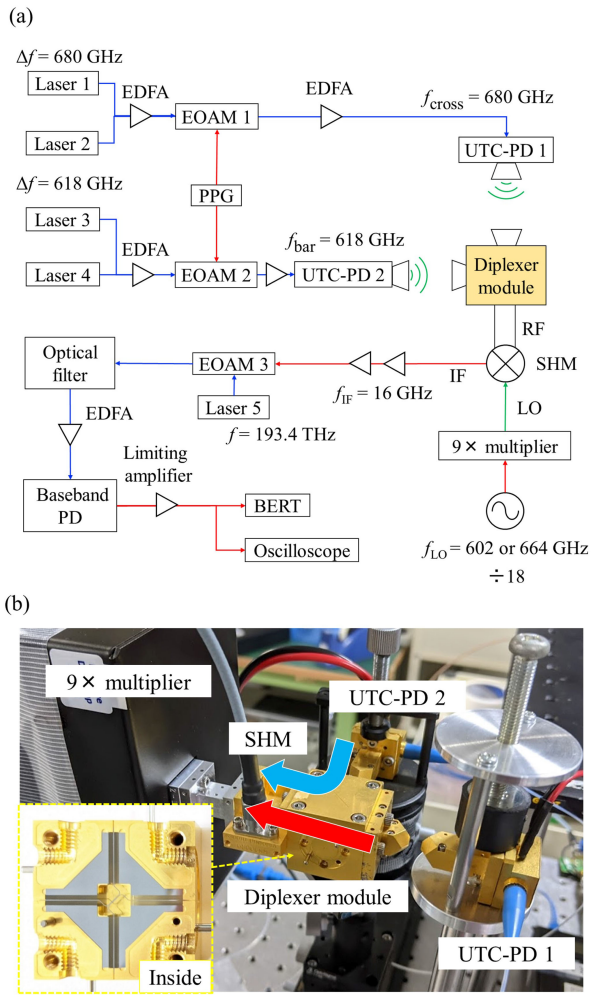

Fig. 11. Proof-of-concept wireless communication system for the developed diplexer module. (a) Block diagram of the two-channel wireless communication experiment using the developed diplexer module in the 600-GHz band. Blue, red, and green line denote optical signal, electric signal, and THz signal, respectively. (b) Photographs of the experimental setup and inside view of the developed diplexer module.

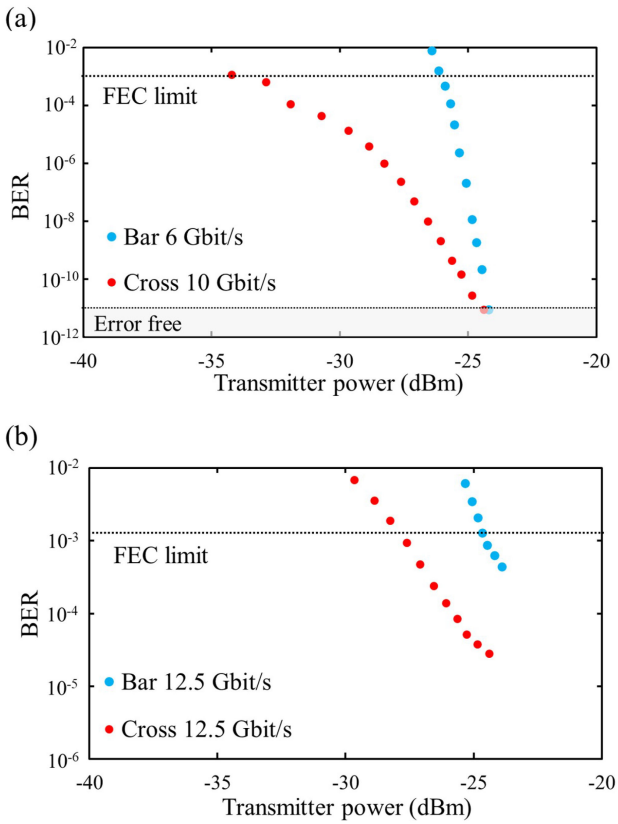

Fig. 12. Results of the two-channel wireless communication experiments using the Si diplexer module in the 600-GHz band. Blue and red denote bar and cross directions, respectively. (a) BER characteristics at the highest error-free communication speed, 10 Gbit/s in the cross direction and 6 Gbit/s in the bar direction. (b) BER characteristics at the maximum communication speed under the FEC limitation, 12.5 Gbit/s in both bar and cross directions.

received by the horn antennas attached to the module ports corresponding to ports 3 and 2 in Fig. 5(a), and then combined by the diplexer module. The module port corresponding to port 1 of the Si diplexer module in Fig. 5(a) is connected to the SHM, and these combined waves are injected into the SHM that acts as the heterodyne Rxs to achieve higher sensitivity than the envelope detectors, as shown in Fig. 11(b). The wireless communication distance was set to approximately 1 cm in both directions for the proof-of-concept experiment.

The system for Rx was the same as that described in Section III-B. Since there is only one SHM for 600-GHz band in our lab, the data are acquired by switching the LO frequency such that each IF frequency is 16 GHz (i.e., f_{LO}= 602 GHz in the bar direction and f_{LO}= 664 GHz in the cross direction), while the carrier signals at 680 and 618 GHz are transmitted from the two UTC-PDs continuously. The signal demodulated by the baseband PD was shaped by a limiting amplifier, and the BER and eye diagrams were measured using a BERT and oscilloscope, respectively.

B. Result

Fig. 12(a) shows that error-free communication of up to 10 Gbit/s in the cross direction and 6 Gbit/s in the bar direction was achieved, as indicated by the circled dots. The eye pattern shown in Fig. 13(a) and (b) opens clearly and no noise is observed, indicating error-free transmission.

In addition, we achieved a data rate of up to 12.5 Gbit/s on both channels, which is the maximum data rate that can be output from the PPG used in this experiment, and was under the forward error correction (FEC: BER of less than 2.0×10^{-3}[52]) limit, as shown in Fig. 12(b). The eye patterns shown in Fig. 13(e) and (f) show a lot of noise between the eye openings, and the maximum BER measured by BERT were 2.8×10^{-5} and 4.4×10^{-4} in the cross and bar directions, respectively. The major factor in limiting the BER characteristics is the low signal-to-noise ratio, which is due to the low transmit power of UTC-PDs, up to –23.9 dBm. In the future, it could be possible to increase the output power by improving the elements and the internal circuit of the UTC-PD module, and by performing spatial power synthesis [53] in the cross and bar directions, respectively. Furthermore, other methods, such as increasing the IF frequency or introducing an equalizer after the SHM to pseudoenhance the IF bandwidth of the SHM can be used.

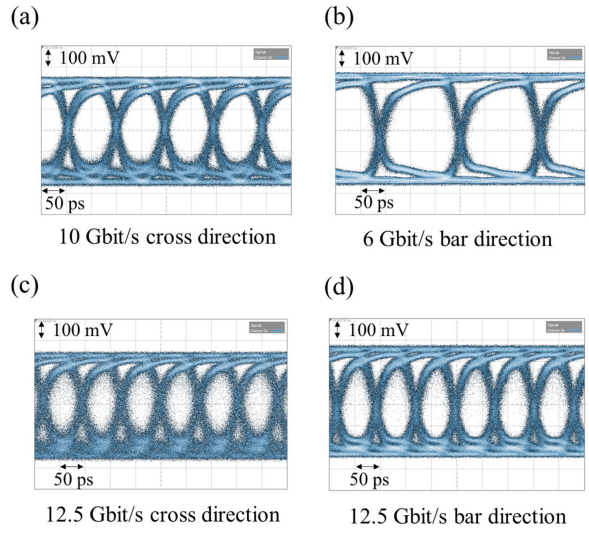

Fig. 13. Demodulated eye diagrams of the two-channel wireless communication experiment using the Si diplexer module in 600-GHz band. (a) Two-channel transmission at data rate of 10 Gbit/s in the cross direction. (b) Two-channel transmission at data rate of 6 Gbit/s in the bar direction. (c) Two-channel transmission at data rate of 12.5 Gbit/s in the cross direction. BER $= 2.8 \times 10^{-5}$. (d) Two-channel transmission at data rate of 12.5 Gbit/s in the bar direction. BER $= 4.4 \times 10^{-4}$.

V. Conclusion

In this study, we developed an Si dielectric diplexer and Si dielectric waveguide packaging module for FDM multichannel wireless communication in the THz band and demonstrated its operation by transmission characteristic measurements and wireless communication experiments in the 600-GHz band.

A packaging module for Si dielectric waveguides with WR1.5 standard metallic hollow waveguides was developed and successfully operated with an insertion loss of about 0.2 dB, while maintaining the low-loss characteristics of the dielectric waveguide technology.

Furthermore, we designed an Si dielectric diplexer, which is a key device for FDM communication. The coupling length L and coupling separation S of the diplexer are optimized to improve the crosstalk between the diplexers in the region capable of wireless communication in the 600-GHz band, which eliminates the negative impact caused by channel crosstalk. We succeeded in achieving an Si dielectric diplexer mounted packaging module with a 3-dB bandwidth of 101 GHz in the cross direction and 37 GHz in the bar direction. The crosstalk of the diplexer at 680 GHz in the cross direction and 618 GHz in the bar direction were -34 and -41 dB, respectively.

In addition, we performed two-channel wireless communication in the 600-GHz band using the developed Si dielectric diplexer to verify its operation. As a result, error-free wireless communication of up to 10 and 6 Gbit/s could be achieved in the cross and bar directions, respectively. Moreover, under the FEC limitation, 12.5 Gbit/s is achieved on both channels.

In the future, we will attempt to conduct two-channel FDM wireless transmission using two SHM receivers, UTC-PD transmitters, and Si diplexer modules at both the Tx and Rx sides. Additionally, to improve the wireless communication speed in the 600-GHz band, we will improve the performance of the UTC-PD transmitter for higher powers and SHM receiver for higher sensitivity and wider RF/IF bandwidth. In addition to increasing the number of integrated couplers and I/O taper structures in the Si dielectric waveguide circuit, as well as the number of I/O ports in the module, we aim to realize an Si dielectric multiplexer module and then use it to conduct further multichannel FDM wireless communication experiments. Furthermore, the proposed packaging module for the Si dielectric waveguide technology is expected to be applied to the integration of sensing systems using dielectric half mirrors and ultralow loss THz combiners/dividers using Y-junction waveguides and on-chip system integration with THz sources and detectors [54].

Acknowledgment

The authors would like to thank Dr. Jeffrey Hesler of Virginia Diodes, Inc. for providing them with a special SHM for the 600-GHz band.

References

[1] H.-J. Song and T. Nagatsuma, "Present and future of terahertz communications," *IEEE Trans. THz Sci. Technol.*, vol. 1, no. 1, pp. 256–263, Sep. 2011.
[2] T. Kleine-Ostmann and T. Nagatsuma, "A review on terahertz communications research," *J. Infrared, Millimeter, Terahertz Waves*, vol. 32, pp. 143–171, 2011.
[3] T. Nagatsuma *et al.*, "Advances in terahertz communications accelerated by photonics," *Nat. Photon.*, vol. 10, pp. 371–379, 2016.
[4] H. Elayan, O. Amin, B. Shihada, R. M. Shubair, and M. -S. Alouini, "Terahertz band: The last piece of RF spectrum puzzle for communication systems," *IEEE Open J. Commun. Soc.*, vol. 1, pp. 1–32, 2020.
[5] T. Nagatsuma and G. Carpintero, "Recent progress and future prospect of photonics-enabled terahertz communications research," *IEICE Trans. Electron.*, vol. E 98–C, no.12, pp. 1060–1070, 2015.
[6] T. Nagatsuma, K. Kato, and J. Hesler, "Enabling technologies for real-time 50-Gbit/s wireless communications at 300 GHz," in *Proc. 2nd Annu. Int. Conf. Nanoscale Comput. Commun.*, 2015, pp. 1–5.
[7] D. M. Slocum, E. J. Slingerland, R. H. Giles, and T. M. Goyette, "Atmospheric absorption of terahertz radiation and water vapor continuum effects," *J. Quan. Spectrosc. Radiat. Transfer*, vol. 127, pp. 49–63, 2013.
[8] T. Nagatsuma, M. Sonoda, T. Higashimoto, L. Yi, and J. Hesler, "12.5-Gbit/s wireless link at 720 GHz based on photonics," in *Proc. 44th Int. Conf. Infrared, Millimeter, Terahertz Waves*, 2019, pp. 1–2.
[9] T. Nagatsuma *et al.*, "600-GHz-band waveguide-output uni-traveling-carrier photodiodes and their applications to wireless communication," in *Proc. IEEE/MTT-S Int. Microw. Symp.*, 2018, pp. 1180–1183.
[10] Y. Uemura, Y. Kawamoto, N. Shibata, L. Yi, and T. Nagatsuma, "600-GHz-band heterodyne receiver system using photonic techniques," in *Proc. Int. Topical Meeting Microw. Photon.*, 2020, pp. 256–259.
[11] V. Petrov *et al.*, "On unified vehicular communications and radar sensing in millimeter-wave and low terahertz Bands," *IEEE Wireless Commun.*, vol. 26, no. 3, pp. 146–153, Jun. 2019.
[12] H. Yi *et al.*, "Characterization for the vehicle-to-infrastructure channel in urban and highway scenarios at the terahertz band," *IEEE Access*, vol. 7, pp. 166984–166996, 2019.
[13] C. Lin and G. Y. Li, "Indoor terahertz communications: How many antenna arrays are needed?," *IEEE Trans. Wireless Commun.*, vol. 14, no. 6, pp. 3097–3107, Jun. 2015.
[14] C. Lin and G. Y. Li, "Adaptive beamforming with resource allocation for distance-aware multi-user indoor terahertz communications," *IEEE Trans. Commun.*, vol. 63, no. 8, pp. 2985–2995, Aug. 2015.
[15] B. Peng and T. Kürner, "A stochastic channel model for future wireless THz data centers," in *Proc. Int. Symp. Wireless Commun. Syst.*, 2015, pp. 741–745.
[16] R. S. Tucker, G. Eisenstein, and S. K. Korotky, "Optical time-division multiplexing for very high bit-rate transmission," *J. Light. Technol.*, vol. 6, no. 11, pp. 1737–1749, Nov. 1988.
[17] Y. Dong, L. Chen, and X. Bao, "Time-division multiplexing-based BOTDA over 100 km sensing length," *Opt. Lett.*, vol. 36, pp. 277–279, 2011.

[18] F. Ren *et al.*, "Cascaded mode-division-multiplexing and time-division-multiplexing passive optical network based on low mode-crosstalk FMF and mode MUX/DEMUX," *IEEE Photon. J.*, vol. 7, no. 5, Oct. 2015, Art. no. 7903509.
[19] S. Berdagué and P. Facq, "Mode division multiplexing in optical fibers," *Appl. Opt.*, vol. 21, pp. 1950–1955, Jun. 1982.
[20] R. Ryf *et al.*, "Mode-division multiplexing over 96 km of few-mode fiber using coherent 6×6 MIMO processing," *J. Light. Technol.*, vol. 30, no. 4, pp. 521–531, Feb. 2012.
[21] W. Zhang *et al.*, "Mode division multiplexing communication using microwave orbital angular momentum: An experimental study," *IEEE Trans. Wirel. Commun.*, vol. 16, no. 2, pp. 1308–1318, Feb. 2017.
[22] K. Kitayama, "Code division multiplexing lightwave networks based upon optical code conversion," *IEEE J. Sel. Areas Commun.*, vol. 16, no. 7, pp. 1309–1319, Sep. 1998.
[23] H. Harada, K. Sato, and M. Fujise, "A radio-on-fiber based millimeter-wave road-vehicle communication system by a code division multiplexing radio transmission scheme," *IEEE Trans. Intell. Transp. Syst.*, vol. 2, no. 4, pp. 165–179, Dec. 2001.
[24] N. Wada and K. Kitayama, "A 10 Gb/s optical code division multiplexing using 8-chip optical bipolar code and coherent detection," *J. Light. Technol.*, vol. 17, no. 10, pp. 1758–1765, Oct. 1999.
[25] J-W. Goossens, M. I. Yousefi, Y. Jaouën, and H. Hafermann, "Polarization-division multiplexing based on the nonlinear Fourier transform," *Opt. Exp.*, vol. 25, pp. 26437–26452, Oct. 2017.
[26] Z. Y. Chen *et al.*, "Use of polarization freedom beyond polarization-division multiplexing to support high-speed and spectral-efficient data transmission," *Light Sci. Appl.*, vol. 6, Feb. 2017, Art. no. e16207.
[27] N. Oshima, K. Hashimoto, S. Suzuki, and M. Asada, "Terahertz wireless data transmission with frequency and polarization division multiplexing using resonant-tunneling-diode oscillators," *IEEE Trans. THz Sci. Technol.*, vol. 7, no. 5, pp. 593–598, Sep. 2017.
[28] N. Karl, R. McKinney, Y. Monnai, R. Mendis, and D. M. Mittleman, "Frequency-division multiplexing in the terahertz range using a leaky-wave antenna," *Nature. Photon.*, vol. 9, pp. 717–720, Sep. 2015.
[29] D. Deslandes and K. Wu, "Integrated microstrip and rectangular waveguide in planar form," *IEEE Microw. Wireless Compon. Lett.*, vol. 11, no. 2, pp. 68–70, Feb. 2001.
[30] R. N. Simons and G. E. Ponchak, "Modeling of some coplanar waveguide discontinuities," *IEEE Trans. Microw. Theory Tech.*, vol. 36, no. 12, pp. 1796–1803, Dec. 1988.
[31] R. Chan and J. Guo, "Analytical modeling of proximity and skin effects for millimeter-wave inductors simulation and design in nano Si CMOS," in *Proc. IEEE MTT-S Int. Microw. Symp.*, 2014, pp. 1–4.
[32] T. Higashimoto, T. Kurokawa, M. Sonoda, and T. Nagatsuma, "Design and characterization of power combiner in 600-GHz band," in *Proc. IEICE Gen. Conf.*, 2018, Art. no. C-14-7.
[33] N. Shibata *et al.*, "600-GHz-Band silicon dielectric waveguide Module," in *Proc. Int. Conf. Infrared, Millimeter Terahertz Waves*, 2021, pp. 1–2.
[34] K. M. K. H. Leong *et al.*, "WR1.5 Silicon micromachined waveguide components and active circuit integration methodology," *IEEE Trans. Microw. Theory Tech.*, vol. 60, no. 4, pp. 998–1005, Apr. 2012.
[35] X. Shang, Y. Tian, M. J. Lancaster, and S. Singh, "A SU8 micromachined WR-1.5 band waveguide filter," *IEEE Microw. Wirel. Compon. Lett.*, vol. 23, no. 6, pp. 300–302, Jun. 2013.
[36] O. Glubokov, X. Zhao, J. Campion, U. Shah, and J. Oberhammer, "Micromachined bandpass filters with enhanced stopband performance and q-factor of 950 at 700 GHz," in *Proc. IEEE MTT-S Int. Microw. Symp.*, 2021, pp. 204–206.
[37] K. Tsuruda, M. Fujita, and T. Nagatsuma, "Extremely low-loss terahertz waveguide based on silicon photonic-crystal slab," *Opt. Exp.*, vol. 23, pp. 31977–31990, 2015.
[38] M. Yata, M. Fujita, and T. Nagatsuma, "Photonic-crystal diplexers for terahertz-wave applications," *Opt. Exp.*, vol. 24, pp. 7835–7849, 2016.
[39] K. Okamoto *et al.*, "Terahertz sensor using photonic crystal cavity and resonant tunneling diodes," *J. Infrared Milli. Terahz. Waves*, vol. 38, pp. 1085–1097, 2017.
[40] D. Headland, W. Withayachumnankul, R. Yamada, M. Fujita, and T. Nagatsuma, "Terahertz multi-beam antenna using photonic crystal waveguide and Luneburg lens," *APL Photon.*, vol. 3, 2018, Art. no. 126105.
[41] W. Gao *et al.*, "Effective-medium-cladded dielectric waveguides for terahertz waves," *Opt. Exp.*, vol. 27, pp. 38721–38734, 2019.
[42] X. Yu, M. Sugeta, Y. Yamagami, M. Fujita, and T. Nagatsuma, "Simultaneous low-loss and low-dispersion in a photonic-crystal waveguide for terahertz communications," *Appl. Phys. Exp.*, vol. 12, Jan. 2019, Art. no. 012005.
[43] D. Headland, W. Withayachumnankul, X. Yu, M. Fujita, and T. Nagatsuma, "Unclad microphotonics for terahertz waveguides and systems," *J. Light. Technol.*, vol. 38, pp. 6853–6862, 2020.
[44] Y. Yang *et al.*, "Terahertz topological photonics for on-chip communication," *Nat. Photon.*, vol. 14, pp. 446–451, 2020.
[45] R. Kakimi, M. Fujita, M. Nagai, M. Ashida, and T. Nagatsuma, "Capture of a terahertz wave in a photonic-crystal slab," *Nature Photon.*, vol. 8, pp. 657–663, 2014.
[46] W. Withayachumnankul, R. Yamada, M. Fujita, and T. Nagatsuma, "All-dielectric rod antenna array for terahertz communications," *APL Photon.*, vol. 3. 2018, Art. no. 051707.
[47] A. V. Subashiev and S. Luryi, "Modal control in semiconductor optical waveguides with uniaxially patterned layers," *J. Light. Technol.*, vol. 24, pp. 1513–1522, 2006.
[48] T. Ishibashi, Y. Muramoto, T. Yoshimatsu, and H. Ito, "Unitraveling-carrier photodiodes for terahertz applications," *IEEE J. Sel. Topics Quantum Electron.*, vol. 20, no. 6, pp. 79–88, Nov./Dec. 2014.
[49] K. Takiguchi, "Method for converting high-speed and spectrally efficient terahertz-wave signal into optical signal," *Opt. Exp.*, vol. 29, no. 5, pp. 6598–6606, 2019.
[50] S. Boscolo, M. Midrio, and C. G. Someda, "Coupling and decoupling of electromagnetic waves in parallel 2D photonic crystal waveguides," *IEEE J. Quantum Electron.*, vol. 38, no. 1, pp. 47–53, Jan. 2002.
[51] D. Headland, X. Yu, M. Fujita, and T. Nagatsuma, "Near-field out-of-plane coupling between terahertz photonic crystal waveguides," *Optica*, vol. 6, pp. 1002–1011, 2019.
[52] I. P. Kaminow, T. Li, and A. E. Willner, *Optical Fiber Telecommunications*. New York, NY, USA: Elsevier2013.
[53] M. P. DeLisio and R. A. York, "Quasi-optical and spatial power combining," *IEEE Trans. Microw. Theory Tech.*, vol. 50, no. 3, pp. 929–936, Mar. 2002.
[54] X. Yu, R. Yamada, J. Kim, M. Fujita, and T. Nagatsuma, "Integrated circuits using photonic-crystal slab waveguides and resonant tunneling diodes for terahertz communication," in *Proc. Prog. Electromagnetics Res. Symp.*, 2018, Art. no. 599–605.

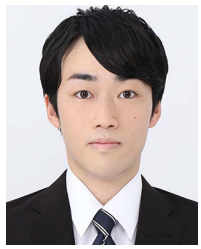

Norihiko Shibata (Student Member, IEEE) received the B.E and M.E degrees in engineering science from Osaka University, Osaka, Japan, in 2020 and 2022, respectively.

Since 2022, he has been with R&D Center, Sony Group Inc., Atsugi, Kanagawa. His research interests include the development of THz silicon photonics devices, and the their application of THz wireless communication and imaging.

Mr. Shibata was the recipient of the Electronics Society Student Award of Institute of Electronics, Information and Communication Engineers, in 2022.

Yuta Uemura (Student Member, IEEE) received the B.E and M.E degrees in engineering science from Osaka University, Osaka, Japan, in 2020 and 2022, respectively.

Since 2022, he has been with NTT DOCOMO Inc., Tokyo, Japan. His research focuses on the development of photonics-based terahertz wireless communication.

Yuma Kawamoto received the B.S. degree in engineering science in 2020 from Osaka University, Osaka, Japan, where he is currently working toward the M.S. degree with the Graduate School of Engineering Science.

His research focuses on the integration and packaging of THz devices for wireless communications.

Li Yi (Member, IEEE) received the B.Sc. degree in geophysics from the School of Ocean and Earth Science, Tongji University, Shanghai, China, in 2011, and the M.E. and Ph.D. degrees in environmental studies from the Graduate School of Environmental Studies, Tohoku University, Sendai, Japan, in 2014 and 2017, respectively.

Then, he was a Researcher with the National Institute of Advanced Industrial Science and Technology, Tokyo, Japan, until 2018. He is currently an Assistant Professor with the Graduate School of Engineering Science, Osaka University, Osaka, Japan. His research interests include photonic-based millimeter/terahertz waves devices and applications, which include imaging and sensing techniques, wireless communication, and signal processing techniques.

Dr. Yi was the recipient of the Student Paper Competition Prize of URSI Japan Radio Science Meeting 2015, President Award of environmental study of Tohoku University in 2017, and Young Scientists Award of IEICE, SANE, in 2018. He is a Member of the Institute of Electronics, Information and Communication Engineers (IEICE), Japan, and currently an Associate Editor for the *IEICE Electronics Express*.

Masayuki Fujita (Member, IEEE) received the Ph.D. degree in ultrasmall and ultralow-threshold microdisk lasers from Yokohama National University, Yokohama, Japan, in 2002.

Subsequently, he joined the Department of Electronic Science and Engineering, Kyoto University, Kyoto, Japan. In 2011, he joined Osaka University, Toyonaka, Japan, and was appointed the Research Director of the Strategic Basic Research Program CREST, "Development of terahertz integrated technology platform through fusion of resonant tunneling diodes and photonic crystals" from 2015 to 2021 and has been the Research Director "Development of integrated devices and systems to control time domain and space distribution of terahertz waves," since 2021 of the Japan Science and Technology Agency. He is currently an Associate Professor with the Graduate School of Engineering Science, Osaka University. His research interests include photonic crystals, including spontaneous emission control in photonic crystals and high-efficiency light extraction in light-emitting diodes, and silicon light emitters, terahertz materials, devices, systems, and photonic nanostructures, microstructures, and their applications.

Dr. Fujita is a Member of the Japan Society of Applied Physics (JSAP), Laser Society of Japan (LSJ), Institute of Electronics, Information and Communication Engineers (IEICE), Japan, Japanese Photochemistry Association, and Optica, formerly OSA. From 1999 to 2002 and from 2003 to 2006, he was a Research Fellow of the Japan Society for the Promotion of Science. He is currently a Vice Chair of the IEICE Technical Committee on Microwave Photonics and Terahertz Photonic-Electronics Technologies, Japan. He was the recipient of various awards, including the IEEE Lasers and Electro-Optics Society Japan Chapter Student Award in 2000, JSAP Young Scientist Presentation Award in 2000, Electronic Material Symposium Award in 2005, JSAP Young Scientist Award in 2006, Research Foundation of Opto-Science and Technology Award in 2007, Paper Award from the LSJ in 2007, and Osaka University Presidential awards for Encouragement in 2013–2015.

Tadao Nagatsuma (Fellow, IEEE) received the B.S., M.S., and Ph.D. degrees in electronic engineering from Kyushu University, Fukuoka, Japan, in 1981, 1983, and 1986, respectively.

In 1986, he joined the Electrical Communications Laboratories, Nippon Telegraph and Telephone Corporation (NTT), Atsugi, Japan. From 1999 to 2002, he was a Distinguished Technical Member with NTT Telecommunications Energy Laboratories. From 2003 to 2007, he was a Group Leader with NTT Microsystem Integration Laboratories, and was an NTT Research Professor from 2007 to 2009. Since 2007, he has been with Osaka University, Osaka, Japan, where he is currently a Professor with the Division of Advanced Electronics and Optical Science, Department of Systems Innovation, Graduate School of Engineering Science. His research interests include ultrafast electronics and millimeter-wave and terahertz photonics.

Dr. Nagatsuma is a Fellow of the Institute of Electronics, Information and Communication Engineers (IEICE), Japan, and the Electromagnetics Academy. He is currently an Associate Editor for the IEEE PHOTONICS TECHNOLOGY LETTERS and the IEEE TRANSACTIONS ON TERAHERTZ SCIENCE AND TECHNOLOGY, the Vice President of the Terahertz Systems Consortium, and was the past Vice President of the IEICE. He was the recipient of numerous awards including the 1989 IEICE Young Engineers Award, 1992 IEEE Andrew R. Chi Best Paper Award, 1997 Okochi Memorial Award, 1998 Japan Microwave Prize, 2000 Ministers Award of the Science and Technology Agency, 2002 and 2011 Asia-Pacific Microwave Conference Prize, 2004 YRP (Yokosuka Research Park) Award, 2006 Asia-Pacific Microwave Photonics Conference Award, 2006 European Microwave Conference Prize, 2007 Achievement Award presented by the IEICE, 2008 Maejima Award, 2011 Recognition from Kinki Bureau of Telecommunications, Ministry of Internal Affairs and Communications, 2011 Commendation for Science and Technology by the Ministry of Education, Culture, Sports, Science and Technology, 2014 IEEE Tatsuo Ito Award, and 2020 Distinguished Achievement and Contributions Award by the IEICE.